

Curvature-dependent metastability of the solid phase and the freezing-melting hysteresis in pores

Oleg Petrov and István Furó

Division of Physical Chemistry, Department of Chemistry, Royal Institute of Technology, SE-10044 Stockholm, Sweden

(Received 15 February 2005; revised manuscript received 28 September 2005; published 31 January 2006)

We recapitulate and generalize the concept of the freezing-melting hysteresis that attributes this phenomenon to a free-energy barrier between metastable and stable states of pore-filling material. In a phenomenological description, we show that under commonly encountered conditions, this renders the freezing-point depression ΔT_f defined by the surface-to-volume ratio S/V , whereas the melting-point depression ΔT_m by the mean curvature κ of the pore surface, with $\Delta T_m/\Delta T_f=2\kappa(V/S)$. Employing ^1H NMR cryoporometry, we experimentally demonstrate the linear correlation between ΔT_m and ΔT_f for several liquids with different $\Delta T_{f,m}$ imbedded in controlled pore glasses. The results compare favorably to the morphological properties of the glasses determined by other techniques. Our findings suggest a simple method for analyzing the pore morphology from the observed phase transition temperatures.

DOI: [10.1103/PhysRevE.73.011608](https://doi.org/10.1103/PhysRevE.73.011608)

PACS number(s): 68.08.-p, 61.43.Gt, 64.70.Dv, 68.35.Rh

I. INTRODUCTION

Because of their high acquired surface-to-volume ratio S/V , small particles or wetting materials confined in small pores melt and crystallize at temperatures well below their bulk melting point T^0 [1,2]. Solid-solid [3] and glass [4] transitions are known to be similarly affected. Ultimately, this behavior is caused by the presence of surface that, compared to bulk, introduces excess energy for the solid and, thereby, shifts the liquid-solid equilibrium toward the liquid state. It can be shown [5] that, for condensed phases (liquid and solid), the excess energy is equal to the total surface free energy that is, in turn, proportional to S/V . The shift of the solid-liquid equilibrium point T_{eq} is conventionally evaluated via a characteristic pore size

$$T_{eq} - T^0 = - \frac{v \gamma_{sl} T^0}{\Delta H} \frac{1}{(\text{pore size})}, \quad (1)$$

where γ_{sl} is the surface free energy [$\text{J} \times \text{m}^{-2}$] of the solid-liquid interface, v the molar volume, and ΔH the latent heat of melting. Equation (1) is referred to as the Gibbs-Thomson equation by analogy with that well known from the nucleation theory [5]. There is, however, a long history and a rich variation in the literature as concerning the exact dependence of the temperature shift on pore dimensions in Eq. (1) (see, for example, Refs. [2,6,7]). One of the reasons for this diversity and disagreement lies with different approaches to determining the excess energy; in Sec. II we consider this point in more detail.

It has also long been known that freezing within pores occurs at a lower temperature than melting; the phenomenon is called the freezing-melting hysteresis [3,7–23]. Despite its direct bearing on a wide spectrum of phenomena (such as frost damage [24], frost heave in soil [25,26], ice formation in microorganisms and tissues [27], and cryo- and thermoporometry [7,11,15,23,28–31]), the precise nature of the hysteresis remains, at present, controversial, all the more so as authors consider different conditions under which freezing occurs [28,32]. There are three major avenues for rationalizing the freezing-melting hysteresis. The first one simply sees

the hysteresis as an uncontrollable delay by homogenous nucleation on cooling, well known for bulk liquids (binodal versus spinodal) [3,28,33]. The second family of explanations associates the hysteresis to pore-blocking effects on penetration of a solid front into pores; the simplest version of this approach is the so-called ink-bottle mechanism of hysteresis [20,25,29]. The third concept, less directly but also related to the solid front propagation, attributes the hysteresis to a free-energy barrier, which separates metastable states of a confined material from stable ones [6,34–38]. This concept is related to the earlier approach by Broekhoff and de Boer to gas adsorption-desorption hysteresis [39]. A validity of assumptions and range of conditions under which a particular mechanism of hysteresis predominates are not fully explored and require additional study.

In the present work, we recapitulate and generalize the third concept of the hysteresis. We show that under commonly encountered conditions, the hysteresis can be readily explained by different paths along which solid-liquid interface propagates during freezing and melting. Within this approach, the hysteresis is considered as a result of pore curvature-induced metastability of the solid phase and, thereby, is an intrinsic property of the system defined by the pore morphology and the interfacial interactions. In Sec. II, we develop a simple phenomenological model of the freezing-melting hysteresis for an open-ended pore. The model employs a formalism of equidistant surfaces, which allows us to express the free energy of a confined system as a function of a single parameter for an arbitrarily shaped pore. In Sec. III, we experimentally verify the predictions of the model by using several different liquids confined in controlled pore glasses (CPG). In Sec. IV, we also discuss some experimental results from the literature that are clarified in our description.

II. THEORY

Consider an arbitrarily shaped pore with volume V and surface S that is filled by a solid core surrounded by a liquid layer of width t , as shown in Fig. 1(a). We assume that the

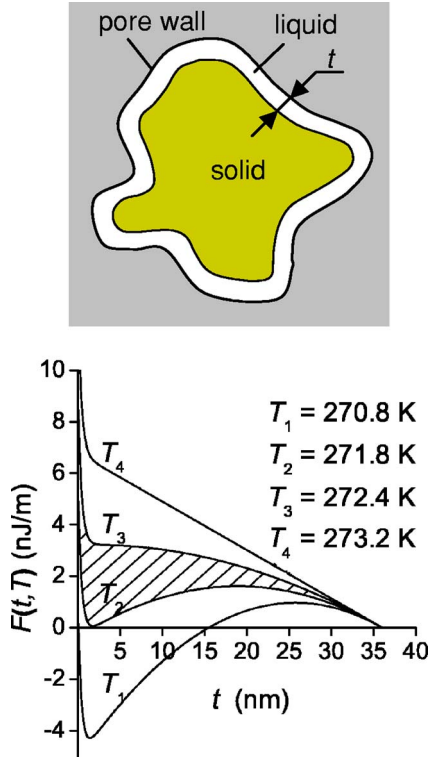


FIG. 1. (Color online) (a) Cross-sectional view of a pore filled by a solid core and a liquid layer of uniform width t . (b) The free energy of water for a unit length of a cylindrical pore of 36 nm radius as function of t and temperature T , as provided by Eq. (4) with $\Delta\gamma \approx \gamma_{sl} = 30$ mJ/m² [63,64] and $\xi = 0.4$ nm (roughly two molecules thick). The metastable region providing the freezing-melting hysteresis is hatched.

liquid wets the pore wall and that the pore is sufficiently large for the pore-filling material to have thermodynamically well-defined and single-valued properties. Hence, pore sizes in the order of a nanometer or less are beyond our treatment and more accessible to simulation studies [40,41]. The Helmholtz free energy of the system is [6,35–38]

$$F = \frac{\mu_s V_s}{v_s} + \frac{\mu_l (V - V_s)}{v_l} + \gamma_{sl} S_s + \gamma_{lw} S + \Delta\gamma S e^{-t/\xi} - p_s V_s - p_l (V - V_s). \quad (2)$$

We use the Helmholtz potential because there is a curvature dependence of pressure $p_{s,l}$ associated with solid (s) and liquid (l) interfaces, so phase transitions in the system are not necessarily isobaric. On the other hand, we neglect changes in volume of the system upon phase transitions. Hence, it is the Helmholtz free energy that seeks a minimum for the system to be in equilibrium. The first two terms in Eq. (2) are the volume free energies of the solid and liquid phases, $\mu_{s,l}$ their chemical potentials, and $v_s \approx v_l = v$, and the next two terms the free energies of the solid-liquid (sl) and liquid-wall (lw) interfaces. The exponential term accounts for the short-range ($\sim \xi$) surface-induced perturbation in the liquid [42,43]. $\Delta\gamma \equiv \gamma_{sw} - (\gamma_{sl} + \gamma_{lw})$ is the free energy that a solid-wall interface has in excess over a liquid-covered wall in

contact with the solid core (for wetting liquids $\Delta\gamma > 0$ [43–45]).

Further evaluation requires two considerations. First, the free energy of incompressible materials cannot depend on the pressure and, thereby, any pressure (including the pressure exerted by the curved interface) dependence of the various terms in Eq. (2) must cancel [5,36]. The validity of this assumption also depends on the magnitude of difference between v_s and v_l and the pore size that defines the magnitude of the excess pressure; hence, the absence of significant pressure terms can be experimentally tested (see Sec. III). Second, since the temperature dependence of the chemical potential [5,36,38] is in first order

$$\mu_s - \mu_l = \Delta H (T - T^0) / T^0, \quad (3)$$

the t -dependent part of F becomes

$$F(t, T) = \frac{\Delta H T - T^0}{v} V_s(t) + \gamma_{sl} S_s(t) + \Delta\gamma S e^{-t/\xi}. \quad (4)$$

$F(t, T)$ is illustrated in Fig. 1(b) for a water-filled cylindrical pore. At low temperatures, it has two local minima: the minimum at $t = r$ corresponds to a pore filled by liquid, while the minimum at $t = \tau(\xi, T) \approx 0$ to a pore that is, except the nonfreezing film of width τ , filled by solid. This film between the solid core and pore wall is a direct consequence of the short-range ($\sim \xi$) surface-induced perturbation, and its existence at temperatures far below the bulk freezing point has been amply demonstrated [43,46–49]. The presence of this nonfreezing film at the pore surface is a fact of crucial importance for our model.

The energy barrier between the minima reflects the competition between volume and surface contributions to F ; a well-known analogy exists in nucleation theory [5]. Consider here the temperature dependence of $F(t, T)$. By starting from the frozen state at T_1 and increasing temperature, we reach the solid-liquid equilibrium point T_2 , where the two corresponding minima of F are equally deep. However, melting cannot occur at this temperature because growing the liquid phase from the nonfreezing film at the pore wall would advance the liquid-solid front along increasing t . Since this has a free-energy penalty, melting will not start until approximately T_3 , where thermal fluctuations are sufficient to surmount the energetic barrier [50]. This temperature is hence associated with the melting point of pore solid, $T_m = T_3$, while from T_2 to T_3 the pore filled with solid is metastable. Upon cooling down from T_4 , where the pore is filled by liquid, the freezing temperature depends on whether solidification takes place in the presence of preexisting crystallites adjacent to the pore or it requires supercooling and nucleation. Under the former condition (i.e., no nucleation barrier), the material freezes at the equilibrium point $T_f = T_2$. This condition may be encountered if one uses an excess (outside but in contact with the pores) of material so that solid can be first formed out of the pore space. Since we do so here, we refer to T_2 as the freezing temperature T_f .

T_f and T_m so defined can be expressed by using conditions for the extrema and inflection point of $F(t, T)$, respectively,

$F=0$ and $F'=0$ at $T=T_f$; while $F'=0$ and $F''=0$ at $T=T_m$. This results in

$$T_f - T^0 \equiv \Delta T_f = -\frac{v\gamma_{sl}T^0}{\Delta H} \frac{S_s + \xi S'_s}{V_s + \xi V'_s}, \quad (5a)$$

$$T_m - T^0 \equiv \Delta T_m = -\frac{v\gamma_{sl}T^0}{\Delta H} \frac{S'_s + \xi S''_s}{V'_s + \xi V''_s}, \quad (5b)$$

where functions $S_s=S_s(t)$, $S'_s=S'_s(t)$, etc., are evaluated at $t=\tau$. Although our assumption of a solid-liquid interface equidistant to the pore wall may not be completely valid, we expect no significant effects as long as $\partial S/\partial V \ll 1/\tau$, a condition that must independently prevail for our phenomenological treatment. Note also that the representation of F as a function of a single parameter t , leading to Eq. (5), is valid only in the range of t , where $S_s(t)$ and $V_s(t)$ are well defined [51]. For complex pore shapes (and, in particular, those with concave sections of pore walls), that may limit t to rather small values. Nevertheless, since melting is defined by the behavior of functions $S_s(t)$, $S'_s(t)$, etc., in Eq. (5) at $t=\tau \approx 0$, this representation may suffice for determining ΔT_m . On the other hand, ΔT_f is determined by the free-energy equality in two states of the pore-filling material that is well defined for any pore shape.

For pore sizes much above τ and, hence ξ , lowest-order approximation in Eq. (5) yields

$$\Delta T_f \cong -\frac{v\gamma_{sl}T^0}{\Delta H} \frac{S}{V}, \quad (6a)$$

$$\Delta T_m \cong -\frac{v\gamma_{sl}T^0}{\Delta H} \frac{\partial S}{\partial V}. \quad (6b)$$

In contrast to previous treatments [6,36–38], Eq. (6) is applicable to any particular pore geometry with competitive volume and surface contributions to the free energy such that F has a local minimum at $t=\tau$.

Clearly, either of Eqs. (6a) and (6b) reproduces the inverse size dependence in Eq. (1). We remark here that expressions similar to Eq. (6a) are widely used for evaluating pore size distribution but often from ΔT_m instead of ΔT_f ; such an interpretation of the melting point generally leads to a size overestimate. Another inconsistency in the literature is when ΔT_f is defined by Eq. (6b) with $\partial S/\partial V$ term arising as the curvature of a solid-liquid front (instead of the curvature of the pore wall) propagating along a cylindrical pore of radius r [52]. Occasionally, since the corresponding solid-liquid front is hemispherical with $\partial S/\partial V(\text{sphere})=S/V(\text{cylinder})=2/r$, a numerically correct result is obtained.

In numerous works, principally originating from those by Pawlow [53] and Rie [54], the shift of T_{eq} is regarded as an effect of the excess pressure exerted on the system by the curved interfaces. Such an approach exploits the Laplace-Young equation and leads to expressions for T_{eq} analogous to Eq. (6a) but with different numerical factor [7,25,55,56]. We stress that in the case of incompressible phases, there is no net work done by pressure, which thereby cannot change the

TABLE I. Properties of CPGs as supported by the manufacturer (Millipore Corporation).

Label	d_0^a (nm)	V^b ($10^{-6} \text{ m}^3/\text{g}$)	S/V (10^6 m^{-1})	φ^c
CPG237	23.7	0.95	82.9	0.68
CPG729	72.9	0.75	33.2	0.62

^aMean pore diameter.

^bSpecific pore volume.

^cPorosity.

free energy upon changing surface area [36]. In other words, the excess energy and the shift of T_{eq} are caused by molecular interactions, including the short-range ($\sim \xi$) perturbation, in the interface region while cohesive interactions in the core may be treated as unaffected by the surface. Hence, under the conditions considered here excess-pressure-related treatments [7,55,56] cannot yield correct results. We do not discuss here three-phase models [28,53,57], where T_{eq} is assumed to be a solid-liquid-vapor equilibrium point (a triple point), which is not obtained in our case.

Using Steiner's formula for equidistant surfaces (see the Appendix), one can rewrite Eq. (6b) as

$$\Delta T_m = -\frac{v\gamma_{sl}T^0}{\Delta H} 2\kappa = \Delta T_f \frac{2\kappa V}{S}, \quad (7)$$

where κ is the integral mean curvature of pore surface, $\kappa = (1/2S)\int_S(1/r_1 + 1/r_2)dS$, with the principal radii of curvature r_1 and r_2 . This result has several important implications. Since for any pore $2\kappa < S/V$ ($2\kappa V/S = 2/3$ for a spherical and $2\kappa V/S = 1/2$ for a cylindrical pore, while $\kappa = 0$ for planar surfaces), one obtains a freezing-melting hysteresis with $\Delta T_m < \Delta T_f$. On the other hand, for a material with the value of $v\gamma_{sl}T^0/\Delta H$ known, Eqs. (6a) and (7) provide two different parameters of morphology, S/V and κ . Even with unknown material properties, Eq. (7) enables a qualitative analysis of pore morphology by evaluating $\Delta T_m/\Delta T_f = 2\kappa V/S$ and comparing this ratio to that for model geometries.

III. EXPERIMENT

We have tested Eq. (7) under experimental conditions that closely correspond to our initial assumptions. Controlled pore glasses (CPGs) [58] made into porous grains ($\sim 120\text{--}150 \mu\text{m}$) with nominal pore diameters of 23.7 and 72.9 nm (referred to below as CPG237 and CPG729, respectively, with properties in Table I) were selected for our experiments. Because of the relatively large ($\gg \xi$) pores, materials confined in them retain their thermodynamic constants measured in bulk [30,59]. Four liquids, all wetting, have been used for filling the CPGs: water, benzene, cyclohexane, and cyclooctane, with a wide spread of values of $v\gamma_{sl}T^0/\Delta H$ (Table II). To measure ΔT_m and ΔT_f , we have employed NMR cryoporometry [46,60,61]. A particular liquid was added to ~ 20 mg of CPG placed in an NMR tube, always with some (15–30%) excess over the amount required for the pore saturation. Then the tube was sealed and centrifuged

TABLE II. Physical properties of the liquids used. Unless otherwise stated, data have been taken from the Crossfire Gmelin database.

Liquid	Formula	v (cm ³ /mol)	Δv^a (%)	T^0 (K)	γ_{sl} (mJ/m ²)	ΔH (kJ/mol)	Dipole moment, D
Water	H ₂ O	18.1	9.2	273.2	30 ^b	6.01	1.9
Benzene	C ₆ H ₆	89.5	-13	278.8	15-44 ^c	9.87	$\sim 10^{-3}$
Cyclohexane	C ₆ H ₁₂	108.7	-6.7	279.9	4.6 ^c	2.63	0.28
Cyclooctane	C ₈ H ₁₆	134.5	-7	287		1.99	

^aVolume expansion upon freezing at T^0 , $(v_s - v_l)/v_l$, from Ref. [71].

^bReferences [63,64].

^cReference [30], and references therein.

during 4 h to remove possible air plugs in pores and promote liquid penetration. Besides suppressing supercooling (see below), the excess material provided the bulk melting point; that is, in-sample temperature calibration.

The NMR measurements were carried out on a Bruker DMX200 spectrometer with a BVT-3000 temperature controller. The integral intensity of the ¹H NMR signal of the liquid phase was measured as a function of temperature as the sample was warmed or cooled. To separate this signal from that of solid, a T_2 -filter was used based on the Carr-Purcell-Meiboom-Gill (CPMG) spin-echo pulse sequence [61] with a relaxation delay of 4-40 ms, depending on the liquid.

The temperature course during the experiment was as follows. The sample was initially cooled to $T=240$ K to get all the liquid frozen and then warmed up to slightly below the respective T^0 , so that the bulk material outside the grains remained frozen. Thereafter, the samples were cooled down with a small decrement (0.1 K in the liquid-solid transition region and 0.5-1.0 K far from that). The measurements were performed with a long-enough (≥ 10 min) waiting time at any temperature to achieve equilibrium. When the liquid fraction was no longer detectable, the temperature was lowered down to $T=240$ K and then raised slowly to record the melting path.

Changes in the liquid signal intensity under different cooling conditions are illustrated in Fig. 2. Clearly, the initial freezing is nucleation controlled: the sample had to be supercooled down to 260 K for any of the bulk or confined water to freeze (upper curve in Fig. 2). The temperature at which freezing commenced starting from an "all-liquid" condition varied between separate experiments on the same CPG; this is another hallmark of nucleation control. But if the excess bulk water was kept frozen, the confined liquid would freeze (lower curve in Fig. 2) at exactly reproducible temperatures as defined by Eq. (6a).

Note that our cooling-warming rates ≤ 0.1 K/(10 min) in the transition regions were at least two orders of magnitude slower than those in comparable calorimetric studies [6,7,11,15,23,28,29]. As another kinetic aspect, CPGs possess a multiconnected pore space. Moreover, there are a multitude [$\sim (D/r)^2$, where D and r are the grain and pore sizes, respectively] of starting points for solidification on the grain surface that is in contact with the frozen excess material. Hence, bottleneck blocking [56,62] of most solidification fronts that advance along different network branches does

not prevent some solidification fronts reaching the grain interior.

Typical NMR liquid intensity curves (with the freezing branch corresponding to the lower curve in Fig. 2) resulted from our experiment are shown in Fig. 3. Because of a distribution of pore properties, the phase transitions occur over some temperature range; we define the average transition temperatures by the inflection points of the respective curves. Figure 4 provides the resulting ΔT_m and ΔT_f ; as predicted by Eq. (7), they are linearly correlated and hence must be defined by the same material properties but by different pore characteristics. Comparing the slope values 0.56 for CPG237 and 0.57 for CPG729 to those expected for spheres ($\Delta T_m/\Delta T_f=0.67$) and cylinders ($=0.5$), the average pore is provided as close to cylindrical in accordance with previous results [49] and with their random tube network appearance (Fig. 5). The same linear behavior for the two different pore sizes implicitly also verifies our initial assumption about neglecting excess-pressure-dependent terms in our free-energy expression above (in this context, also note the different signs of molar volume change for water and the other liquids, Table II).

From the experimental ΔT_f and $\gamma_{sl}=30 \times 10^{-3}$ J/m² for water [63,64] (that has, among our materials, the most reli-

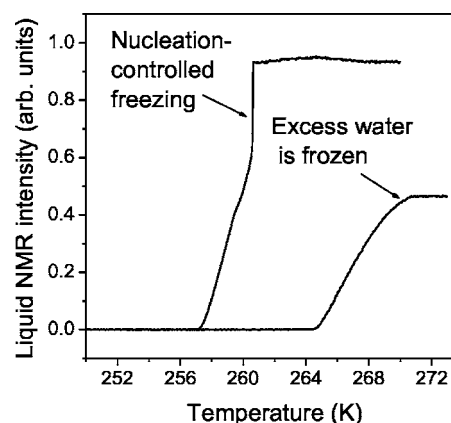


FIG. 2. Illustration of changes in the liquid signal intensity in CPG237 filled with water with 100% excess to the pore volume, as recorded on cooling at a constant rate of 0.04 K/s. Note that this rate is much higher than that used for acquiring the data in Fig. 3. Upper curve: both confined and excess water are initially in the liquid state and freezing is nucleation controlled with corresponding supercooling. Lower curve: excess water is frozen, and therefore, no nucleation is required for the pore water to freeze.

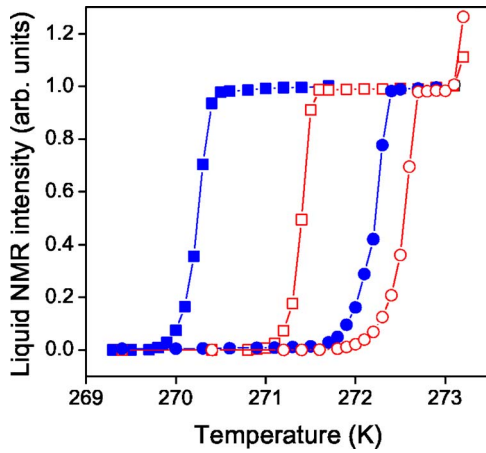


FIG. 3. (Color online) Freezing-melting hysteresis of water confined in controlled pore glasses of 23.7 nm (CPG237, ■) and 72.9 nm (CPG729, ●) average diameters. The solid and open symbols denote the cooling and heating branches, respectively. Unlike Fig. 2, the transitions occur upon quasiequilibrium conditions.

able value of γ_{sl}), Eq. (6a) provides $S/V=120 \times 10^6 \text{ m}^{-1}$ and $38 \times 10^6 \text{ m}^{-1}$ for CPG239 and CPG729, respectively. These values are close to the figures specified by the manufacturer from Brunauer-Emmett-Teller (BET)-type analysis of nitrogen adsorption data (see Table I). The resulting integral mean

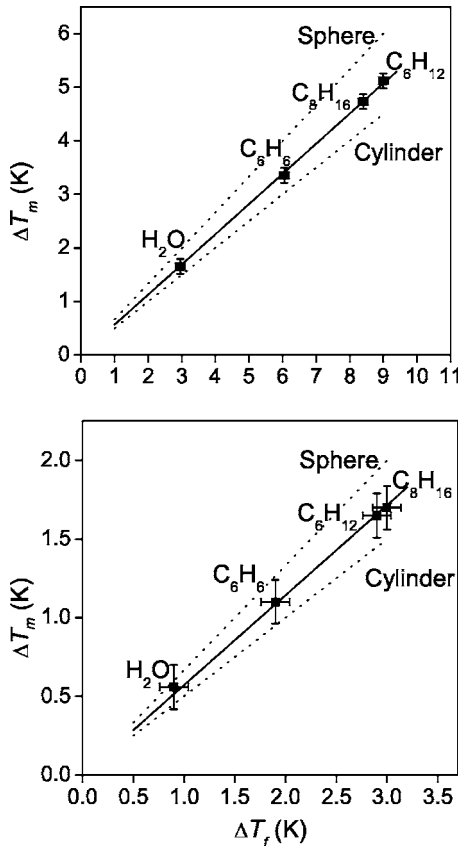


FIG. 4. The relationships between ΔT_f and ΔT_m for four liquids imbibed in controlled pore glasses CPG237 (a) and CPG729 (b). The solid line is a linear fit with zero intercept, and the dashed lines are predictions for cylindrical and spherical pores.

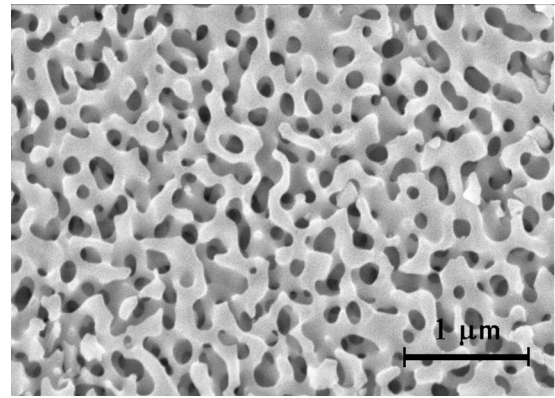


FIG. 5. Electron micrograph of a controlled porous glass from Millipore Corporation (courtesy of Millipore Corporation).

curvatures of CPG239 and CPG729 become $\kappa=35 \times 10^6 \text{ m}^{-1}$ and $11 \times 10^6 \text{ m}^{-1}$, respectively.

IV. DISCUSSION AND CONCLUSIONS

Equation (6) states that T_f and T_m are sensitive to different aspects of pore morphology, namely, T_f to the surface-to-volume ratio while T_m to the curvature of the pore surface. The physical meaning of this result can be illustrated for a cylindrical pore. Upon freezing, liquid solidifies along the pore from the end where the liquid was in contact with bulk solid. Because the changes in the volume and surface energy terms are the same at every step of solidification, there is no energy barrier to surmount and freezing is nonlocal over a continuous volume defined as a pore. The only condition for that pore to freeze is a total reduction of the free energy that is controlled by a parameter global to the pore (S/V). On the other hand, melting is initiated at the liquid film at the pore surface [43,45] and propagates from the surface toward the pore bulk. Up to T_m , the free-energy gradient at the solid-liquid interface is locally unfavorable for melt propagation; thus, melting is controlled by a parameter local to the surface ($\partial S/\partial V$).

We take the good agreement between the S/V values of CPG obtained here from ΔT_f and those from BET-type analysis as a strong support for our model. An independent test is provided by the melting behavior of metal films of 30–100 nm widths [65,66]. In contrast to grains [34,66,67] where ΔT_m depends, as expected, on the inverse of grain size, such films show no significant melting-point depression, as predicted by Eq. (6) applied to planar surfaces with $\kappa=0$. Similarly, our results provide an explanation for the independence of the melting (but not the freezing) temperature of the degree of pore filling [19,30,68]. Finally, the linear correlation between ΔT_m and ΔT_f , which we have demonstrated here, is also valid (though not evaluated that way) for data obtained for water confined in porous silica materials (see Tables 4 and 2 in Refs. [11,19], respectively).

Our findings not only clarify the procedures for obtaining pore size from freezing-melting behavior, but also suggest a simple method for analyzing the pore morphology solely from phase-transition temperature data. In particular, evalu-

ating $\Delta T_m/\Delta T_f=2\kappa V/S$ can provide valuable information on pore shape that is, at present, available only either from model-dependent computer simulations of gas-adsorption experiments or perhaps from combining results of several different experiments, such as mercury intrusion and BET analysis. To our knowledge, only a few, in our opinion incomplete, attempts [6,7,9,11,15,23,29,37,38,62,69] have been, hitherto, made in that direction.

Apart from the methodological aspects, a proper distinction between factors of freezing and melting is important in analysis of a wide spectrum of phenomena with examples of frost damage of building materials [24], intracellular ice formation and freezing injury in microorganisms [27], and frost heave [25,26]. In particular, our results have a bearing on freezing and melting in materials with volume elements in distinct size ranges, such as the pore liquid and the excess liquid, in our case.

ACKNOWLEDGMENTS

This work has been supported by the Swedish Science Council VR. O.P. thanks the Carl Tryggers Stiftelse for financial support.

APPENDIX: STEINER'S FORMULA (BASED ON REFS. [51,70])

Consider a compact surface $\partial\Omega$ enclosing a region Ω . The area S of $\partial\Omega$ is $S=\int_{\Sigma^2}dS=\int_{\Sigma^2}r_1r_2d\sigma$, where $d\sigma$ is an area element of $\partial\Omega$ on its Gaussian map Σ^2 and r_1 and r_2 are the principal radii of curvature. Let $\partial\Omega_t$ be an equidistant surface that consists of points whose oriented distance to $\partial\Omega$ is t . Radii of curvature of $\partial\Omega_t$ are r_1+t and r_2+t . Therefore, with notation $S(t)=S(\partial\Omega_t)$, we obtain

$$S(t)=\int_{\Sigma^2}(r_1+t)(r_2+t)d\sigma=S+2\kappa St+Gt^2,$$

where $\kappa=(1/2S)\int_{\partial\Omega}[(1/r_1)+(1/r_2)]dS$ is the integral mean curvature and $G=\int_{\partial\Omega}(1/r_1r_2)dS$ the integral Gaussian curvature. If V is the volume of Ω and $V(t)$ that of Ω_t , then

$$V(t)=V+\int_{t_0}^t S(t')dt'=V+tS+t^2\kappa S+\frac{1}{3}Gt^3.$$

At $t=\tau\approx 0$, $\partial S/\partial t=2\kappa S$ and $\partial V/\partial t=S$.

-
- [1] J.-P. Borel, *Surf. Sci.* **106**, 1 (1981).
 [2] H. K. Christenson, *J. Phys.: Condens. Matter* **13**, R95 (2001).
 [3] D. D. Awschalom and J. Warnock, *Phys. Rev. B* **35**, 6779 (1987).
 [4] M. Alcoutlabi and G. B. McKenna, *J. Phys.: Condens. Matter* **17**, R461 (2005).
 [5] D. Kashchiev, *Nucleation: Basic Theory with Applications* (Butterworth-Heinemann, Oxford, 2000).
 [6] K. M. Unruh, T. E. Huber, and C. A. Huber, *Phys. Rev. B* **48**, 9021 (1993).
 [7] C. Faivre, D. Bellet, and G. Dolino, *Eur. Phys. J. B* **7**, 19 (1999).
 [8] A. A. Antoniou, *J. Phys. Chem.* **68**, 2754 (1964).
 [9] L. G. Homshaw, *J. Soil Sci.* **31**, 399 (1980).
 [10] B. J.-C. Li, D. K. Ross, and M. J. Benham, *J. Appl. Crystallogr.* **24**, 794 (1991).
 [11] K. Ishikiriyama, M. Todoki, and K. Motomura, *J. Colloid Interface Sci.* **171**, 92 (1995).
 [12] K. Grosse, L. Ratke, and B. Feuerbacher, *Phys. Rev. B* **55**, 2894 (1997).
 [13] M. Sliwinska-Bartkowiak, J. Gras, R. Sikorski, R. Radhakrishnan, L. Gelb, and K. E. Gubbins, *Langmuir* **15**, 6060 (1999).
 [14] B. F. Borisov, E. V. Charnaya, T. Loeser, D. Michel, C. Tien, C. S. Wur, and Y. A. Kumzerov, *J. Phys.: Condens. Matter* **11**, 10259 (1999).
 [15] K. Morishige and K. Kawano, *J. Chem. Phys.* **110**, 4867 (1999).
 [16] K. Morishige and K. Kawano, *J. Phys. Chem. B* **103**, 7906 (1999).
 [17] K. Morishige and K. Kawano, *J. Chem. Phys.* **112**, 11023 (2000).
 [18] J. A. Duffy and M. A. Alam, *Langmuir* **16**, 9513 (2000).
 [19] A. Schreiber, I. Ketelsen, and G. H. Findenegg, *Phys. Chem. Chem. Phys.* **3**, 1185 (2001).
 [20] I. P. Swainson and E. M. Schulson, *Cem. Concr. Res.* **31**, 1821 (2001).
 [21] V. P. Soprunyuk, D. Wallacher, P. Huber, K. Knorr, and A. V. Kityk, *Phys. Rev. B* **67**, 144105 (2003).
 [22] K. Morishige, H. Uematsu, and N. Tateishi, *J. Phys. Chem. B* **108**, 7241 (2004).
 [23] B. V. Enüstün, B. W. Gunnink, and T. Demirel, *J. Colloid Interface Sci.* **134**, 264 (1990).
 [24] C. Hall and W. D. Hoff, *Water Transport in Brick, Stone, and Concrete* (Spon Press, London, 2002).
 [25] D. H. Everett, *Trans. Faraday Soc.* **57**, 1541 (1961).
 [26] J. S. Wettlaufer, *Philos. Trans. R. Soc. London, Ser. A* **357**, 3403 (1999).
 [27] P. Mazur, in *Cryobiology*, edited by H. T. Meryman (Academic Press, London, 1966), p. 213.
 [28] M. Brun, A. Lallemand, J. F. Quinson, and C. Eyraud, *Thermochim. Acta* **21**, 59 (1977).
 [29] E. Molz, A. P. Y. Wong, M. H. W. Chan, and J. R. Beamish, *Phys. Rev. B* **48**, 5741 (1993).
 [30] C. L. Jackson and G. B. McKenna, *J. Chem. Phys.* **93**, 9002 (1990).
 [31] R. Valiullin and I. Furó, *Phys. Rev. E* **66**, 031508 (2002).
 [32] G. W. Scherer, *J. Non-Cryst. Solids* **155**, 1 (1993).
 [33] J. Warnock, D. D. Awschalom, and M. W. Shafer, *Phys. Rev. Lett.* **57**, 1753 (1986).
 [34] S. J. Peppiatt and J. R. Sambles, *Proc. R. Soc. London, Ser. A* **345**, 387 (1975).
 [35] P. R. Couchman and W. A. Jesser, *Nature (London)* **269**, 481 (1977).
 [36] R. R. Vanfleet and J. M. Mochel, *Surf. Sci.* **341**, 40 (1995).

- [37] D. Wallacher and K. Knorr, *Phys. Rev. B* **63**, 104202 (2001).
- [38] R. Denoyel and R. J. M. Pellenq, *Langmuir* **18**, 2710 (2002).
- [39] J. C. P. Broekhoff and J. H. de Boer, *J. Catal.* **9**, 8 (1967).
- [40] F. R. Hung, G. Dudziak, M. Sliwinska-Bartkowiak, and K. E. Gubbins, *Mol. Phys.* **102**, 223 (2004).
- [41] F. R. Hung, B. Coasne, E. E. Santiso, K. E. Gubbins, F. R. Siperstein, and M. Sliwinska-Bartkowiak, *J. Chem. Phys.* **122**, 144706 (2005).
- [42] R. Lipowsky, *Phys. Rev. Lett.* **52**, 1429 (1984).
- [43] J. F. van der Veen, B. Pluis, and A. W. Denier van der Gon, in *Chemistry and Physics of Solid Surfaces*, edited by R. Vanselow and R. F. Howe (Springer, New York, 1988), p. 455.
- [44] J. F. van der Veen, *Surf. Sci.* **433-435**, 1 (1999).
- [45] J. G. Dash, *Rev. Mod. Phys.* **71**, 1737 (1999).
- [46] K. Overloop and L. Van Gerven, *J. Magn. Reson., Ser. A* **101**, 179 (1993).
- [47] J. G. Dash, H. Fu, and J. S. Wettlaufer, *Rep. Prog. Phys.* **58**, 115 (1995).
- [48] T. Ishizaki, M. Maruyama, Y. Furukawa, and J. G. Dash, *J. Cryst. Growth* **163**, 455 (1996).
- [49] R. Valiullin and I. Furó, *J. Chem. Phys.* **117**, 2307 (2002).
- [50] In our example in Fig. 1(b), the mean amplitude of fluctuations in a pore of length L is $\delta F = \sqrt{NkT}$ with $N = 6.02 \times 10^{23} \pi r^2 L / v$. Melting occurs if δF is larger than the barrier height for melting $\Delta F(T)$ where the latter is linearly dependent on L . If we consider $L > 2r$ as necessary for a practical definition of a pore, melting remains hindered up to 0.1 K below T_3 .
- [51] A. Ros, *J. Am. Math. Soc.* **17**, 373 (2003).
- [52] Z. Liu, K. Muldrew, R. G. Wan, and J. A. W. Elliott, *Phys. Rev. E* **67**, 061602 (2003).
- [53] P. Pawlow, *Z. Phys. Chem.* **65**, 1 (1909).
- [54] E. Rie, *Z. Phys. Chem.* **104**, 354 (1923).
- [55] P. Buffat and J.-P. Borel, *Phys. Rev. A* **13**, 2287 (1976).
- [56] G. W. Scherer, *Cem. Concr. Res.* **29**, 1347 (1999).
- [57] K.-J. Hanzen, *Z. Phys.* **157**, 523 (1960).
- [58] T. H. Elmer, *Engineered Materials Handbook* (ASM International, Materials Park, OH, 1992), Vol. 4, p. 427.
- [59] S. J. Gregg and K. S. W. Singh, *Adsorption, Surface Area, and Porosity* (Academic Press, London, 1982).
- [60] J. H. Strange, M. Rahman, and E. G. Smith, *Phys. Rev. Lett.* **71**, 3589 (1993).
- [61] E. W. Hansen, C. Simon, R. Haugsrud, H. Raeder, and R. Bredesen, *J. Phys. Chem. B* **106**, 12396 (2002).
- [62] I. P. Swainson and E. M. Schulson, *Cem. Concr. Res.* **31**, 1821 (2001).
- [63] S. B. Kiselev, *Int. J. Thermophys.* **22**, 1421 (2001).
- [64] P. Taborek, *Phys. Rev. B* **32**, 5902 (1985).
- [65] F. O. Jones and K. O. Wood, *Br. J. Appl. Phys.* **15**, 185 (1964).
- [66] G. L. Allen, R. A. Bayles, W. W. Gile, and W. A. Jesser, *Thin Solid Films* **144**, 297 (1986).
- [67] J. R. Sambles, *Proc. R. Soc. London, Ser. A* **324**, 339 (1971).
- [68] K. Morishige and H. Iwasaki, *Langmuir* **19**, 2808 (2003).
- [69] D. D. Awschalom and J. Warnock, *Phys. Rev. B* **35**, 6779 (1987).
- [70] C. N. Likos, K. R. Mecke, and H. Wagner, *J. Chem. Phys.* **102**, 9350 (1995).
- [71] D. Rozental, *Bull. Soc. Chim. Belg.* **45**, 585 (1936).